TOWARD AN ACCURATE APPROACH FOR THE PREDICTION OF THE FLOW IN A T-JUNCTION: URANS

E. MERZARI*, A. KHAKIM, H. NINOKATA and E. BAGLIETTO[1]
Department of Nuclear Engineering, Tokyo Institute of Technology
Meguro-ku, Ookayama 2-12-2, N1-5 458, Tokyo, Japan
[1] CD-Adapco, Melville, New York
*Corresponding author. E-mail : merzari@nr.titech.ac.jp

Received January 12, 2009
Accepted July 3, 2009

In this study, a CFD methodology is employed to address the problem of the prediction of the flow in a T-junction. An Unsteady Reynolds Averaged Navier-Stokes (URANS) approach has been selected for its low computational cost. Moreover, Unsteady Reynolds Navier-Stokes methodologies do not need complex boundary formulations for the inlet and the outlet such as those required when using Large Eddy Simulation (LES) or Direct Numerical Simulation (DNS). The results are compared with experimental data and an LES calculation. In the past, URANS has been tried on T-junctions with mixed results. The biggest limit observed was the underestimation of the oscillatory behavior of the temperature. In the present work, we propose a comprehensive approach able to correctly reproduce the root mean square (RMS) of the temperature directly downstream of the T-junction for cases where buoyancy is not present.

KEYWORDS : Thermal Hydraulics, T-junction, CFD, URANS

1. INTRODUCTION

Thermal fatigue is a significant long-term degradation mechanism in nuclear power plants. In general, common thermal fatigue issues are well understood, and preventive as well as corrective measures can be taken by relying on plant instrumentation. However, incidents indicate that certain piping system Tees are susceptible to turbulent temperature mixing effects that cannot be adequately monitored through traditional techniques (e.g., common thermocouples).

In fact, temperature fluctuations arise immediately downstream of the area where hot and cold water flows meet in T-junctions, resulting in the repeated thermal loading of the piping structures [1]. Examples of damage due to thermal striping have been reported in mixing Tees of the feedwater systems, reactor water cleanup systems and residual heat removal systems in light water reactor (LWR) power plants. Since the high-cycle thermal fatigue phenomenon due to temperature fluctuation strongly depends on the geometry of the piping and the flow pattern of the liquid, it is difficult to generalize a heuristic evaluation method. A CFD-based methodology able to simulate this inherently unsteady phenomenon is therefore desirable, in order to provide the necessary guidance to design and operation.

The typical computational model used for CFD calculations [2-4] of the flow in a T-junction is shown in Fig. 1. The model includes two short inlet branches where the velocity is imposed and an outlet where the mass flux is imposed to equal the sum of the two inlet fluxes.

Often, downstream of the T-junction, the flow is inherently unsteady; therefore, only unsteady approaches will be considered here. The three main possible approaches to the solution of the unsteady Navier-Stokes equations are Large Eddy Simulation (LES), Direct Numerical Simulation (DNS) and Unsteady Reynolds Averaged Navier-Stokes (URANS). There is also a vast array of mixed approaches combining URANS and LES.

LES and DNS have each been tried with mixed success on this geometry [3]. They are potentially able to predict with considerable accuracy flow distributions such as the velocity profile and the root mean square (RMS) of the velocity components. However, these methods suffer from two fundamental limits:

1. they present a computational cost which grows rapidly with an increasing Reynolds number, and
2. they need complex formulations of the inlet boundary conditions.

In the present work, an Unsteady Reynolds Averaged Navier-Stokes [5] approach has been selected for its lower computational cost. Moreover, Unsteady Reynolds Navier-Stokes methodologies do not need complex boundary formulations for the inlet.

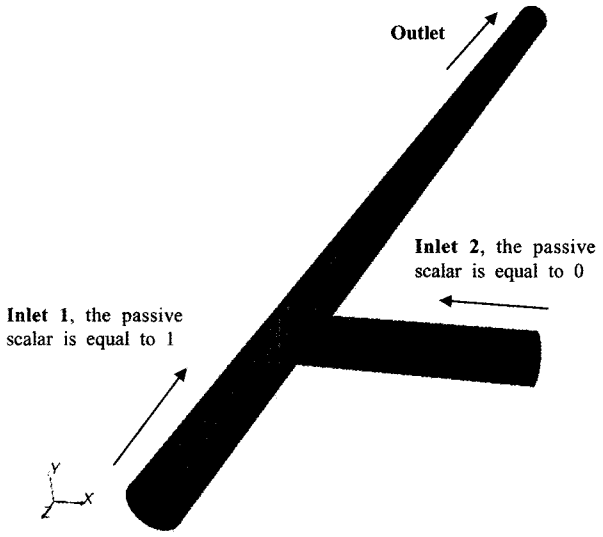

Fig. 1. Computational Model

The outlet boundary condition presents computational problems in itself, and the outlet branch of the T-junction needs to be very long in order for the flow to develop properly. Following [3], the length of the branch in this study has been specified as equal to 20 times the diameter of the tube (although in [3], the length of the branch was actually equal to 25 times the diameter of the pipes).

URANS has also been applied in several cases to the flow in a T-junction, but the results were even less satisfactory than those of the LES and DNS approaches, especially in cases where buoyancy plays a significant role [6]. This is an inherent limit of URANS that cannot be easily addressed. For flows driven by both shear and buoyancy, LES/DNS approaches often remain the only reliable CFD methodologies. For cases where buoyancy is marginal, however, there is no reason to assume that URANS would not be able to reproduce the oscillatory behavior of the temperature.

It is important to point out that it should not be expected that URANS will accurately reproduce the experimental behavior of a temperature time series. In fact, as will be seen below, part of the oscillatory behavior of the temperature must be modeled (Section 2). In fact, URANS tends to under-estimate the amplitude of temperature fluctuations [5]. Despite this well known limit, it will be demonstrated that URANS can be used to correctly predict averaged turbulence statistics such as the average temperature distribution and the RMS of the temperature in the immediate vicinity of the T-junction, if buoyancy is not present. URANS is also able to qualitatively reproduce the frequency spectrum (at low frequencies).

The authors of this study do not intend to advocate the use of URANS as it is formulated here for the problem of thermal fatigue. However, what is presented here could be regarded as the first step toward the definition of a methodology able to address such problem at a limited computational cost.

An additional alternative to a full DNS/LES approach could be given by the use of a coarse LES formulation, as proposed by Merzari *et al.* [7]. Such configuration entails complex boundary conditions (through the introduction of synthetic turbulence at the inlets [8]) and wall modeling to reduce the computational cost. Even though inelegant and inaccurate near the walls, such a formulation has achieved satisfactory results and will be used as an additional comparison for the URANS calculations performed here.

In the present work, we will simulate experimental case Nr. 14, published in [9][1]. The case simulated here is isothermal, but the fluid at the two inlets is characterized by different values of the conductivity. Thus, the mixing can be adequately modeled by the solution of a transport equation for an arbitrary passive (i.e., non-reactive) scalar c representative of the temperature. The choice of this experiment is motivated by:

1. the absence of buoyancy;
2. the detailed RMS plots published by the authors, which permit an assessment of the capability of the code to correctly reproduce the RMS of the passive scalar; and
3. the high resolution.

The diameter of the tube is equal to 0.05 m, the working fluid is water and the Reynolds number on both inlet branches is equal to 25000.

2. A COMPLETE URANS METHODOLOGY

2.1 Mathematical Model

In the present work, the Navier-Stokes equations are solved in their Reynols Averaged form (where the brackets represent ensemble averaging and not temporal averaging):

$$\frac{\partial\langle u_i\rangle}{\partial t}+\langle u_j\rangle\frac{\partial\langle u_i\rangle}{\partial x_j}=-\frac{1}{\rho}\frac{\partial\langle p\rangle}{\partial x_i}-\frac{\partial}{\partial x_j}\left(\tau_{ij}-\nu\frac{\partial\langle u_i\rangle}{\partial x_j}\right), \quad (1.1)$$

$$\frac{\partial\langle u_i\rangle}{\partial x_i}=0 \quad (1.2)$$

where $\tau_{ij}=\langle u_iu_j\rangle-\langle u_i\rangle\langle u_j\rangle$ needs closure.

It represents a fundamental aspect of the mathematical model that is particularly critical in the present configuration since the flow is highly influenced by secondary vortices

[1] Additional experimental data for the same case has been published in [19] and [20].

induced both by velocity gradients (i.e., they are induced by the curvature of the flow at the junction) and by anisotropic turbulence. Since both effects are present (even though the first would certainly be dominant), it is reasonable to use a turbulence model able to reproduce anisotropic turbulence. In the present work, a non-linear cubic relationship will be assumed for the Reynolds stresses τ_{ij}:

$$\rho\tau_{ij} = \frac{2}{3}\rho k\delta_{ij} - \mu_t S_{ij} + C_1\mu_t\frac{k}{\varepsilon}\left[S_{ik}S_{kj} - \frac{1}{3}\delta_{ij}S_{kl}S_{kl}\right] + C_1\mu_t\frac{k}{\varepsilon}\left[\Omega_{ik}S_{kj} - \frac{1}{3}\delta_{ij}\Omega_{jk}S_{ki}\right]$$
$$+C_3\mu_t\frac{k}{\varepsilon}\left[\Omega_{ik}\Omega_{jk} - \frac{1}{3}\delta_{ij}\Omega_{kl}\Omega_{kl}\right] +$$
$$+C_4\mu_t\frac{k^2}{\varepsilon^2}S_{kl}\left[S_{ki}\Omega_{lj} - \frac{1}{3}\delta_{ij}S_{ki}\Omega_{li}\right] + C_5\mu_t\frac{k^2}{\varepsilon^2}S_{ij}\left[S_{kl}S_{kl} - \frac{1}{3}\delta_{ij}S_{kl}\Omega_{kl}\right] \quad (1.3)$$

where S_{ij} is the Strain tensor and Ω_{ij} is the rotation tensor. k (turbulent kinetic energy), $\sum$ (turbulent dissipation) and μ_t (turbulent viscosity) are parameters and are determined by solving two additional transport equations [21]. Details of the model are available in [10] and in appendix A, where the coefficients C_1, C_2, C_3, C_4 and C_5 are defined.

In order to model the mixing in the T-junction, an additional equation is solved for the concentration c of high conductivity fluid. This concentration ranges between 0 (at the inlet of the low conductivity fluid) to 1 (at the inlet of the high conductivity fluid). The transport equation for the passive scalar c can then be written in a URANS approach as:

$$\frac{\partial\langle c\rangle}{\partial t} + \langle u_j\rangle\frac{\partial\langle c\rangle}{\partial x_j} = -\frac{\partial}{\partial x_j}\left(\tau_j^c - \frac{\nu}{\sigma}\frac{\partial\langle c\rangle}{\partial x_j}\right), \quad (2)$$

where σ is the Schmidt number of the fluid and $\tau_j^c = \langle cu_j\rangle - \langle c\rangle\langle u_j\rangle$, which represents a term that needs closure. The following model is usually employed:

$$\tau_j^c = -\frac{\nu_t}{\sigma_t}\frac{\partial\langle c\rangle}{\partial x_j}, \quad (3)$$

where $\nu_t = \frac{\mu_t}{\rho}$ and σ_t is the turbulent Schmidt number for the fluid. Since the objective of the present work is to predict correctly not only the value of the concentration but also the fluctuations, it is necessary to evaluate the RMS of the concentration. This quantity, in a steady state simulation where ensemble averaging and temporal averaging coincide, can be defined as:

$$c_{rms} = \sqrt{\langle(c - \langle c\rangle)^2\rangle}, \quad (4)$$

which, in an URANS simulation, is ill defined and time dependent, since the ensemble averaged concentration is not constant over time. It is thus more coherent to define the fluctuation over the time average, and not the ensemble average, as the sum of two contributions.

$$c^2_{rms} = \overline{\langle(c - \langle c\rangle)^2\rangle} + \overline{(\langle c\rangle - \overline{\langle c\rangle})^2}, \quad (5)$$

where the overbar here represents the operation of averaging over time. The second term, often labelled "coherent," takes into account the contribution to the fluctuation of c given by large-scale structures, i.e. the turbulent structures that are simulated through the URANS simulation. The first term, "incoherent" or "non-coherent," is related to the contribution to the fluctuation of c given by the inherent nature of turbulence. As an example, in isotropic turbulence the second term would be negligible while the first term would be rigorously non-zero near an interface.

The evaluation of the first term can be carried out only through the solution of an additional equation for the transport of the variance of the scalar c. This equation assumes the expression [11]:

$$\frac{\partial\langle c'^2\rangle}{\partial t} + \langle u_j\rangle\frac{\partial\langle c'^2\rangle}{\partial x_j} = -\frac{\partial}{\partial x_j}\left(\tau_j'^c - \frac{\nu}{\sigma}\frac{\partial\langle c'^2\rangle}{\partial x_j}\right) + P - D, \quad (6)$$

where $\overline{\langle c'^2\rangle} = \overline{\langle(c - \langle c\rangle)^2\rangle}$. $\tau_j'^c$ can be modeled in a fashion similar to τ_j^c. P is the production term and D is the dissipation term for the variance of the scalar. P is defined as :

$$P = -2\tau_j'^c\frac{\partial\langle c\rangle}{\partial x_j}, \quad (7)$$

and therefore can be directly computed. The dissipation term D can be traditionally modelled, in equilibrium flows, through:

$$D = C_\chi\frac{\varepsilon}{k}\langle c'^2\rangle, \quad (8)$$

and C_χ has been specified as equal to 1.5, following Warhaft [12]. Since, however, the flow in the junction area is not in equilibrium (i.e., the turbulence is not isotropic), this model might not be particularly accurate. Possible improvements over this model might need to be considered in the future.

2.2 Numerical Practices

The codes used are STAR-CCM+ [13] and STAR-

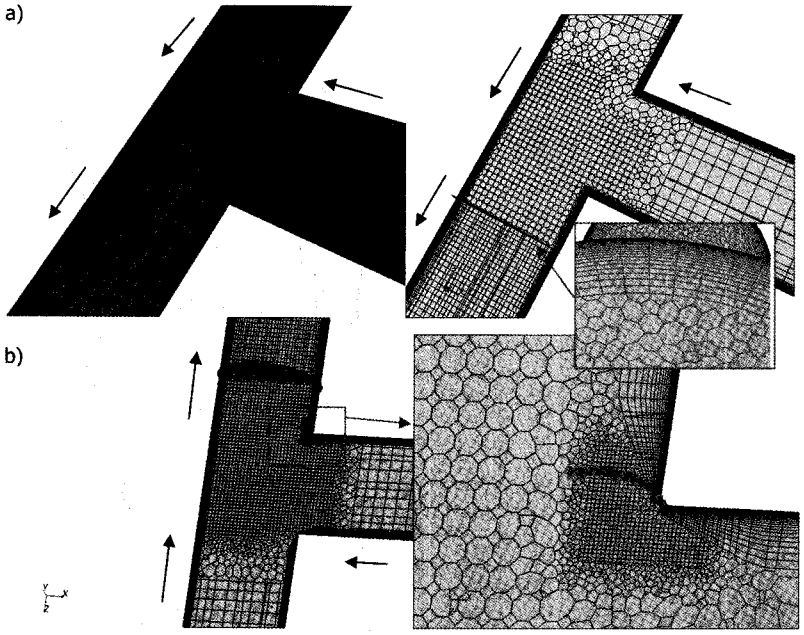

Fig. 2. Coarse Mesh (Top) and Fine Mesh (Bottom). The Black arrows Roughly Represent the Flow Directions

CD 4.06 [14]. The variance equation (6) was implemented only in STAR-CD 4.06. The use of the two different codes was implemented to achieve independent verification of the results. The results for the passive scalar did not differ significantly between the two codes.

In both cases, a polyhedral grid has been used with a prismatic layer near the wall boundary. The wall region has been modelled through a Low-Reynolds model. Two different meshes have been used, a fine grid (approximately 1,000,000 polyhedral meshes) and a coarse grid (approximately 500,000 polyhedral meshes). Images of both meshes are shown in Fig. 2. Steady state calculations have been run on both meshes. Since the difference between the results was not significant, extensive URANS calculation has been run only on the coarse grid. However, to be sure of avoiding any grid-related effects, brief URANS calculations have also been run on the fine grid. The development and shape of the oscillatory behaviour of the passive scalar was found to be independent of the grid type.

The convective fluxes have been discretized through second order upwind schemes in STAR-CCM+ and MARS [14] or central differencing (CD) in STAR-CD. Time advancement has been carried out in both cases through implicit second order schemes with a CFL around 1.0 for STAR-CD and a CFL around 5.0 for STAR-CCM+. The algorithm for STAR-CD was the unsteady SIMPLE algorithm. A segregated approach has also been used in STAR-CCM+. The inlet boundary in all cases has been implemented by imposing the wall law for pipe flow at the inlet.

The PISO algorithm [15], used for preliminary calculations, was found to be inadequate for the present problem. Residuals tend to remain high during the simulation, and this affects the quality of the solution downstream of the T-junction. Moreover, with some turbulence models it has been noticed that the oscillatory behaviour of the passive scalar is not reproduced.

As a preliminary study, several additional turbulence models have also been tested to verify that the unsteadiness observed is not inherent to the Baglietto-Ninokata turbulence model [10]. An unsteady behaviour was observed with all of the models employed, which were:

1. the Spalart-Allmaras model [16];
2. the k-ε Suga Cubic model [17]; and
3. the k-ε standard cubic non-linear model [14].

3. RESULTS

The objective of the present paper is not to provide a complete review of the flow in a T-junction. The focus of this work is to show that, for the simulation to correctly reproduce the scalar and the scalar RMS downstream of a T-junction, it is necessary to do the following:

1. to use URANS (and not RANS) to simulate the unsteady behaviour, and
2. to model the equation of the variance.

Experimental data has been provided only immediately downstream of the T-junction on planes normal to the stream-wise direction that will be referred to as measurement planes 1 (51 mm downstream), 2 (91 mm downstream), 3 (191 mm downstream) and 4 (311 mm downstream).

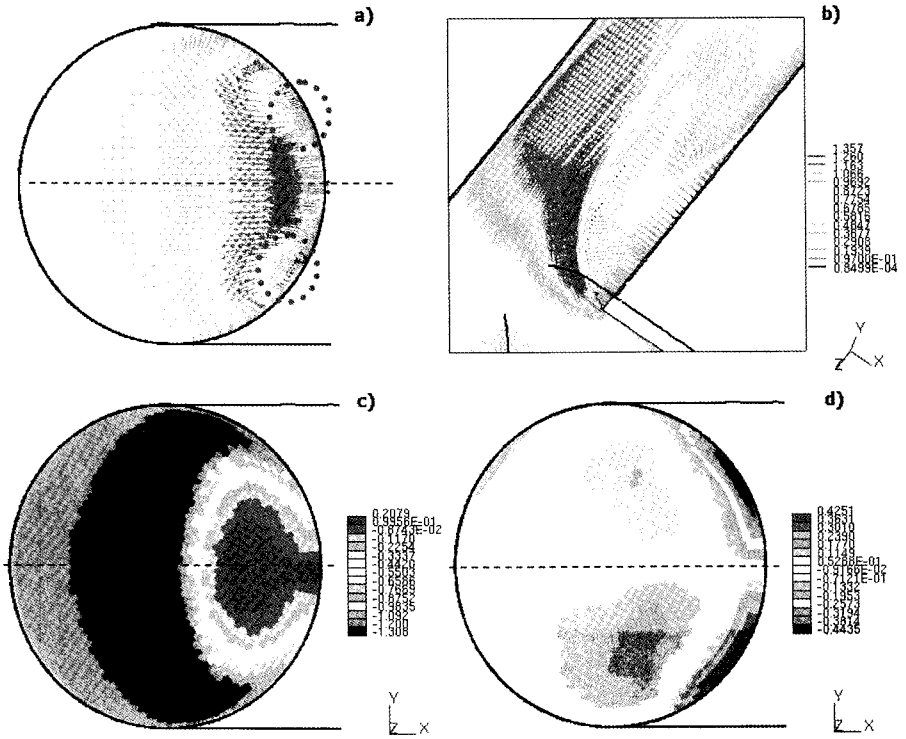

Fig. 3. Averaged Velocity Field Obtained with URANS. (a) Vector Plot Measurement Plane 1, Two Counter-rotating Vortices can be Seen in the Cross Section; (b) Vector Plot on the Symmetry Plane of the System; (c) Streamwise Velocity Distribution on Measurement Plane 1; (d) Distribution of the Velocity in Direction y in Measurement Plane 1. The Dashed Line Represents the Projection of the Symmetry Plane on Measurement Plane 1

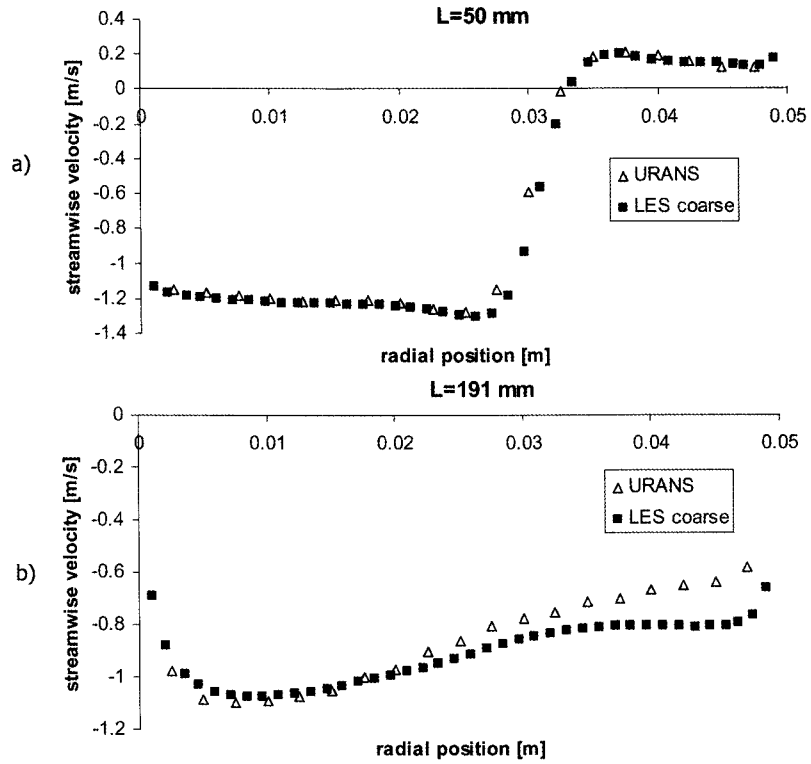

Fig. 4. Comparison for the Velocity Distribution on the Symmetry Axis of Measurement Plane 1 (a) and Measurement Plane 3 (b)

3.1 Brief Review of the Flow Field

In T-junctions where the mass flow rate in the two branches is similar, a couple of strong counter-rotating vortices are present in the outlet pipe immediately downstream of the junction when Reynolds averaging is performed on the flow field [9]. This is well reproduced in the present calculation, as can be seen in Fig. 3. The averaging was performed over 20 s.

The presence of the two vortices can inferred from the contour plots in Fig. 3. Both velocity distributions are non-zero and quasi-symmetrical on the symmetry plane (dashed line in Fig. 3). Since the velocity in direction y has an anti-symmetric distribution (considering the symmetry plane of the T-junction, Fig. 3d) it is evident that a couple of counter rotating vortices are present near the outlet pipe wall (Fig. 3a). The stream-wise velocity distribution has an inversion of sign in the vortex region, and this has significant effects on the distribution of the scalar. It is worth noticing that the averaged stream-wise velocity distribution is fairly different from the experiment [9]. However, the averaging time in the experiment might not be sufficient (since it is reasonable to assume the averaged velocity distributions to be fairly symmetrical). In fact, the instantaneous flow field is very irregular, and the time required to reach full convergence of the averaged statistics is considerable.

An additional comparison can be obtained by comparing the velocity distribution on measurement planes 1 and 4 for LES and URANS (Fig. 4). As can be seen in the figure, URANS obtains results very similar to those of LES at one diameter, while the results tend to be significantly different further downstream.

Figure 5 shows an instantaneous streamline plot downstream of the measurement plane. It can be seen in the figure that some streamlines are oriented backward. Further downstream, at a distance of two diameters to three diameters (2D-3D) from the junction, strong coherent structures develop in the wake of the two vortices. This can be seen on the same plot by the fact that all streamlines tend to oscillate downstream after reaching the region of the coherent structures.

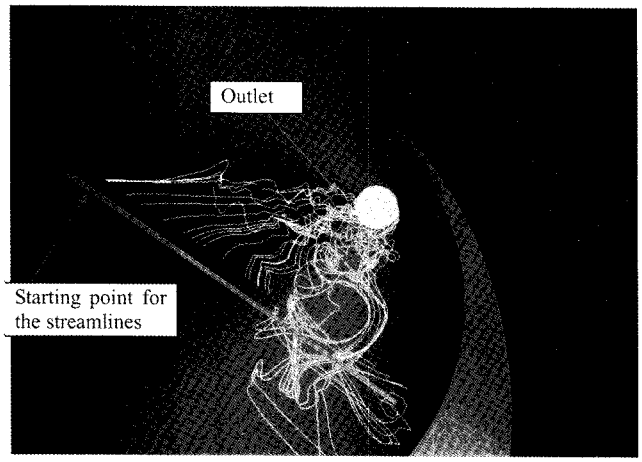

Fig. 5. Instantaneous Streamlines Downstream of the T-junction

3.2 Results for the Scalar

The instantaneous distribution of the passive scalar reflects the presence of coherent structures downstream of the junction (Figure 6 shows a section on the plane parallel to the stream-wise direction for an instantaneous plot of the passive scalar). When compared to the results of the LES of Merzari *et al.* [7], it is evident that, even though the oscillatory behaviour is somehow reduced,

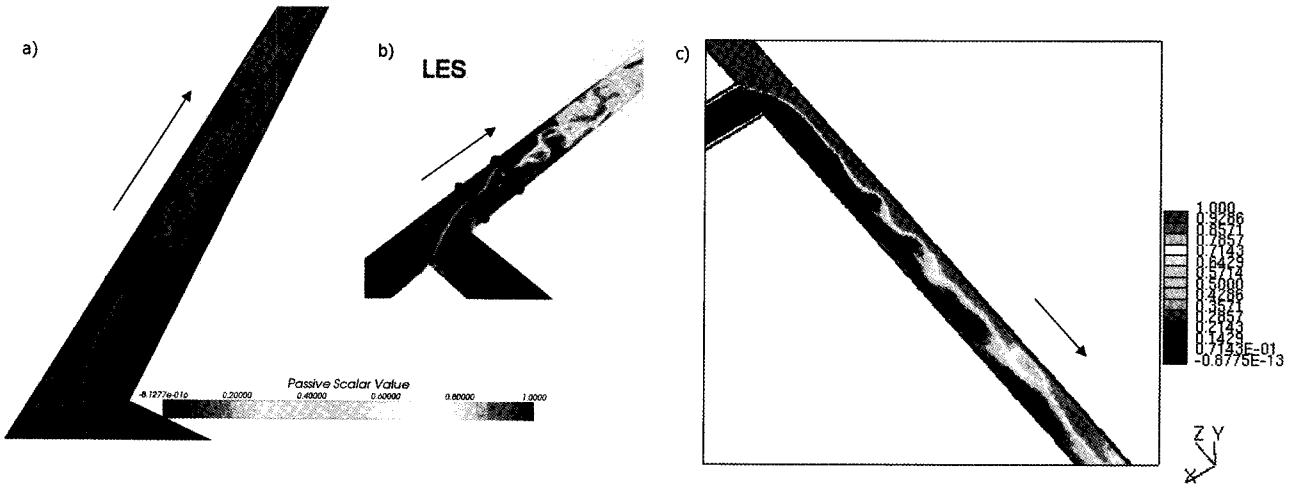

Fig. 6 Instantaneous Contour Plot for the Passive Scalar. (a) URANS Performed on STAR-CCM+; (b) LES on STAR-CCM+: (c) URANS on STAR 4.06. The arrow Represents the Flow Direction

the physics of the phenomenon are captured.

It can be seen that the passive scalar presents a strong oscillating behaviour downstream of the junction, which is indicative of strong vortices. Their presence is highlighted by Q contours (Fig. 7). The function Q is defined in [18] as the second invariant of the velocity gradient tensor:

$$Q = \frac{1}{2}\left(\Omega_{ij}\Omega_{ij} - S_{ij}S_{ij}\right) \quad (9)$$

where Ω_{ij} is the local rotational tensor and S_{ij} the local strain. Positive values of Q indicate regions where vorticity prevails over strain. In previous studies, coherent structures have been identified as surfaces on which Q maintains a

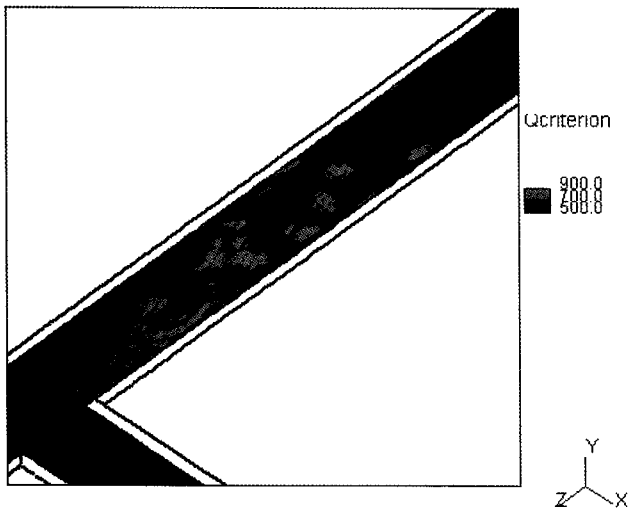

Fig. 7. Instantaneous Plot on the Symmetry Plane of the Q-Factor, the Light Coloured Region Represents the Region with Q> 700 s^{-2}

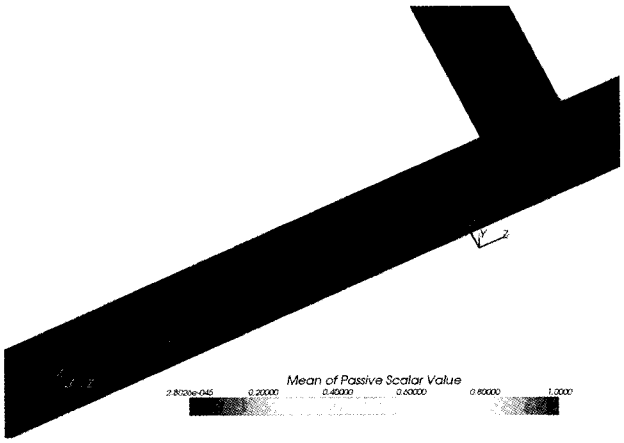

Fig. 8. Averaged Contour Plot for the Passive Scalar

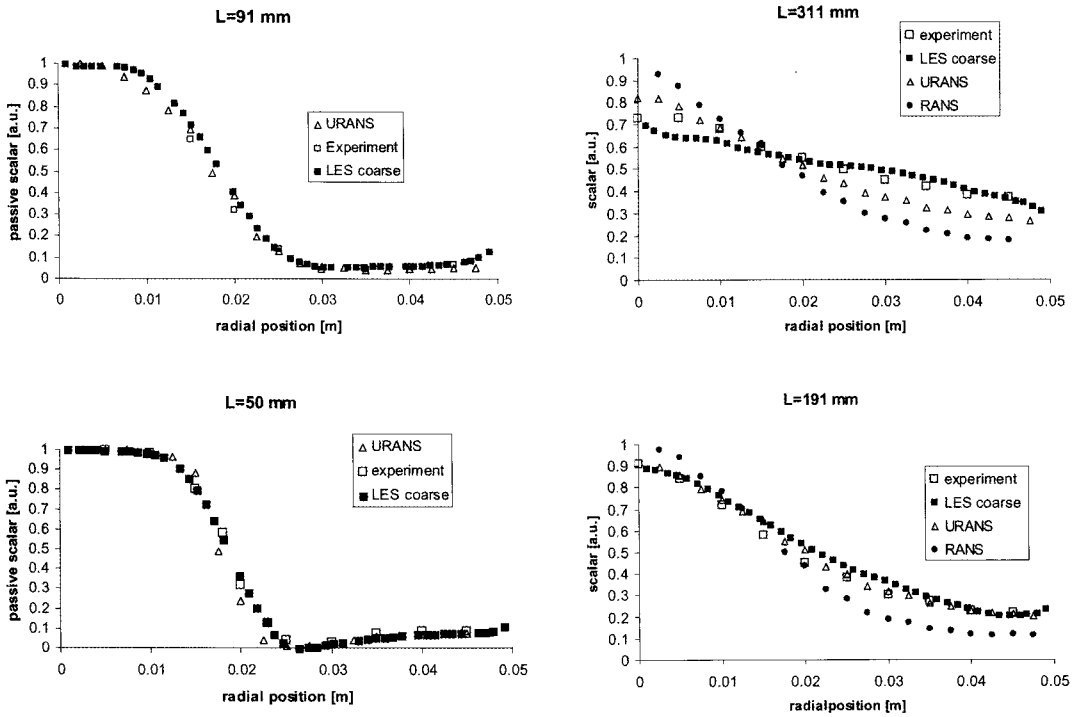

Fig. 9. Averaged for the Passive Scalar on the Symmetry Axis of Measurement Planes 1, 2, 3 and 4

constant positive value (Q> T, where T is an arbitrary threshold). Figure 6 shows the presence of strong positive regions of Q in the wake of the junction. The structures generated near the junction between the pipes eventually reach the interface between the fluids downstream, producing the oscillatory behavior observed in Fig. 5 and enhancing the mixing of the passive scalar.

When Reynolds averaged is applied to the passive scalar, the distribution of c presents a relatively sharp interface between the mixing fluids, up to 2 D downstream of the junction (Fig. 8). However, in the vortex region the averaged value of the scalar is higher than 0 near the wall. This suggests that part of fluid from Inlet 1 is entrained in the vortex region from further downstream [9].

The authors of [9] published detailed experimental results for the passive scalar (available in [19]), and it is therefore possible to compare measurement planes 1, 2, 3 and 4. These results are given in Fig. 9a. Accuracy is deemed acceptable except in the interface region, where the resolution might be insufficient to fully capture the dynamics of the interface. It is also possible that the ensemble average time in the experiment was not sufficient.

Further downstream at about 2D (measurement plane 2), the effect of the coherent structures on the mixing of the scalar becomes self-evident. Figure 9b shows the improvement obtained by employing an URANS approach over a RANS approach. The improvement is more marked downstream, as is clearly shown by Fig. 9c and Fig. 9d on measurement planes 3 and 4.

At about 6D, the agreement between experiment and calculation starts to be less satisfying (Fig. 9d). At this point, the calculation starts to under-estimate the mixing. We believe that the effect is due to a slight deformation of the coherent structures in the present calculation. However, the improvement over RANS is still considerable, and the overall agreement with LES is satisfying up to 4 D downstream of the T-junction.

It is worth noting that in the present calculation the Schmidt number has been kept to the traditional value of 0.9. Frank [19] has reported an improvement in steady state calculations with lower Schmidt numbers (0.1 and 0.2) in the context of an RSM turbulence model. Lower Schmidt numbers tend to artificially smooth the passive scalar distribution. It is possible that, using lower Schmidt numbers, the results shown in Fig. 9 could be significantly improved.

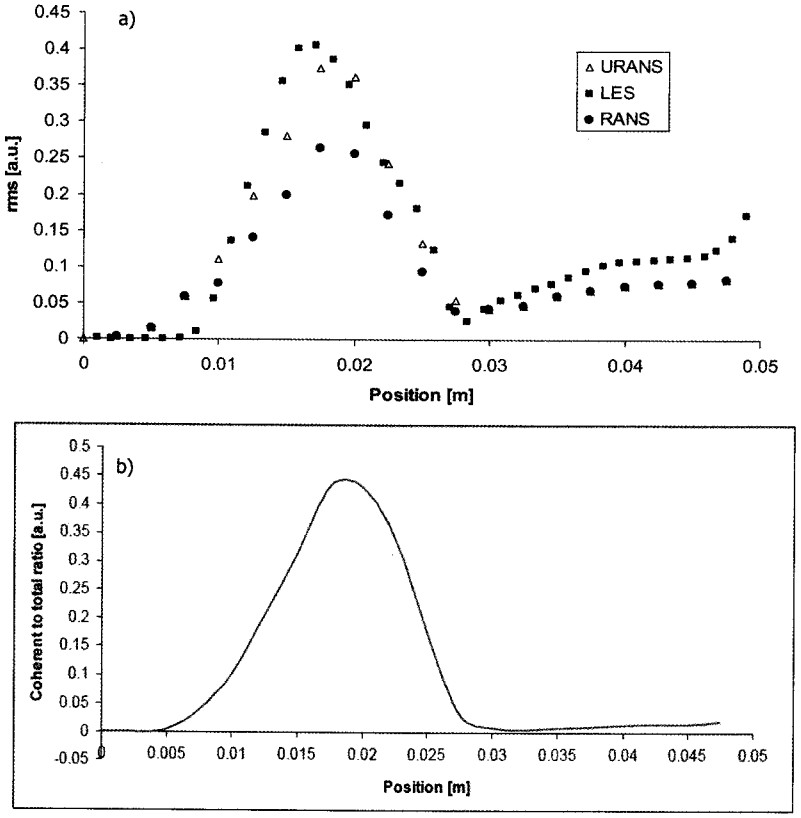

Fig. 10. (a) RMS of the Scalar on the Symmetry Axis of Measurement Plane 1 (51 mm Downstream); (b) Ratio between the Coherent Component of the Variance and the Total Variance on the Symmetry Axis of the Measurement Plane 1 (51 mm Downstream)

3.3 Results for the RMS

The authors of [9] also published a contour plot of the RMS of the passive scalar on measurement plane 1. The peak value of the RMS on the measurement plane was found approximately equal to 0.3 - 0.35 (located near the interface). As discussed in the previous sections, the only way to correctly simulate the RMS of the passive scalar is to consider both contributions to the variance. This has been done in the present study with STAR 4.06 through the use of user subroutines. The averaging in this case has been performed over 2 s and 20.000 time steps.

As can be seen in Fig. 10, the peak of the computed RMS on the symmetry line of measurement plane 1 is equal to 0.35. This is reasonably close to the experimental value. The distribution of the RMS is also in qualitative agreement with the experiment and the LES results. RANS, performed using equation (1.3), grossly underestimated the RMS peak. The position of the RMS peak is approximately 0.008 m from the centre of the outlet pipe in the calculation and approximately 0.007 m in the experiment (this value has been extrapolated from the contour graph in [9]). The incoherent part of the variance dominates in the vortex region (Fig. 10b).

Figure 11 shows how the RMS develops further downstream (91 mm). The RMS profile smoothes, and the contribution of the coherent structures to the oscillation of the passive scalar becomes more homogeneous in the cross section. The agreement with LES data is deemed satisfactory in this case as well.

Fig. 12 shows the contour plot of the variance for both LES and URANS on measurement plane 1. The results are in qualitative agreement with the experiment [9].

Fig. 13 shows the variance distribution of the passive scalar in the cross section for both URANS and LES and L=311 mm (measurement plane 4). The agreement in this region is less satisfactory, and it appears that the non-coherent part of the RMS is dominant (this is an indication that the computation presents a marginal unsteady behaviour in this region).

If a CFD methodology is to be applied successfully to thermal fatigue, it has to predict correctly the RMS of the temperature near the wall. URANS and LES agree on the intensity and location of the maximum variance of the passive on the wall surface (Fig. 14), thus giving us confidence in the capability of such techniques to properly address the T-junction problem in the absence of buoyancy effects.

Due to the poor performance of RANS (Fig. 10 and 11) in the prediction of the RMS, it is possible to conclude that agreement for the RMS can be achieved only if both

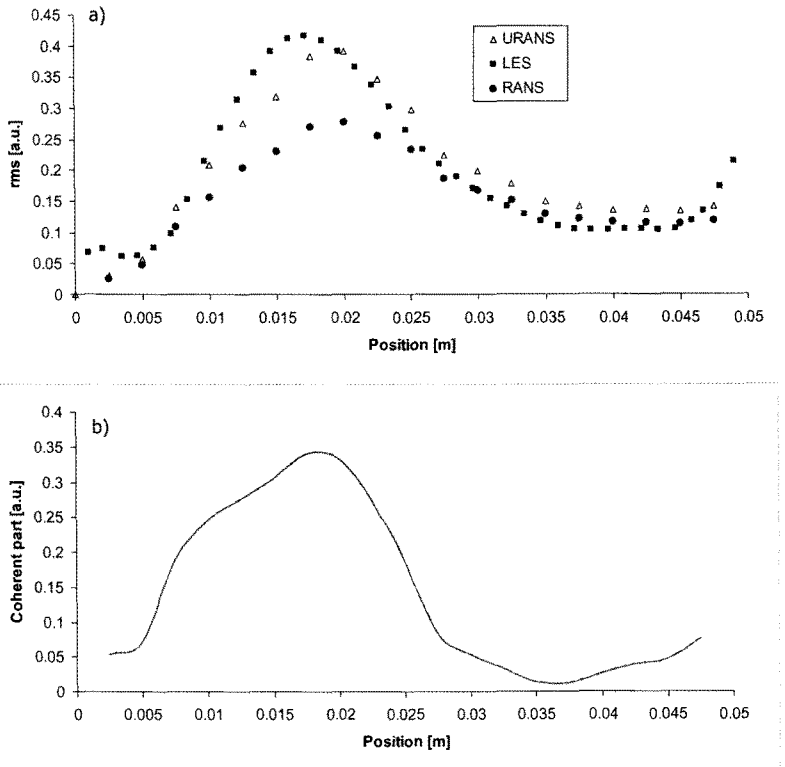

Fig. 11. (a) RMS of the Passive Scalar; (b) Ratio between the Coherent Component of the Variance and the Total Variance on the Symmetry Axis of Measurement Plane 2 (91 mm Downstream)

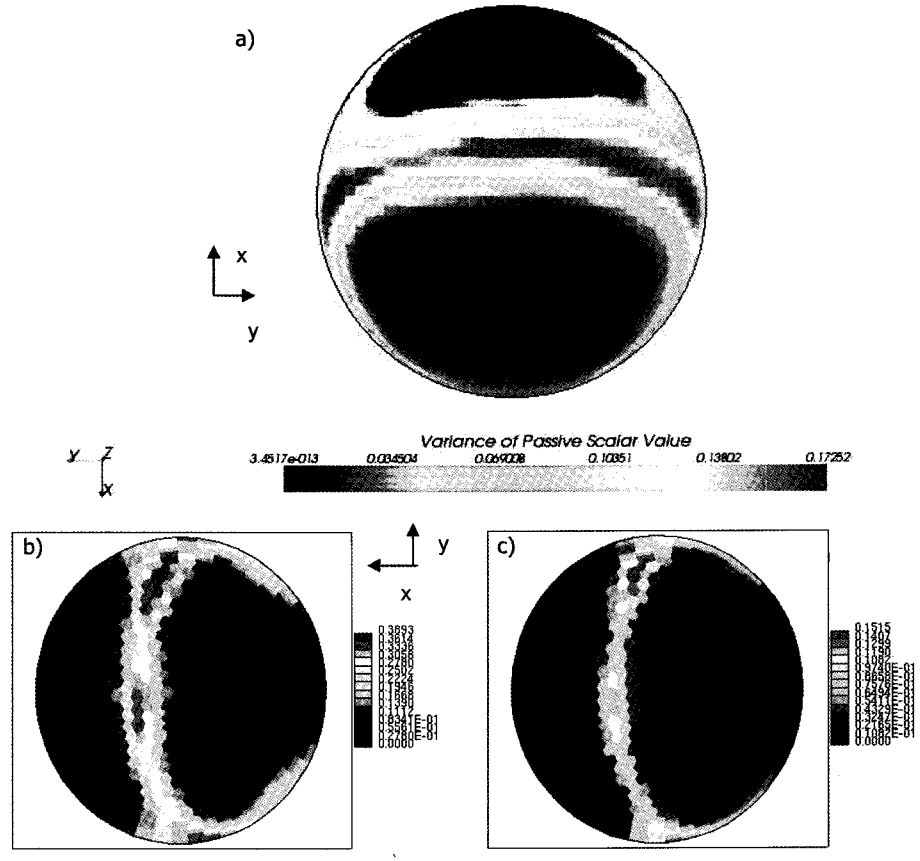

Fig. 12. RMS and Variance of the Passive Scalar on Measurement plane 1: (a) LES (Variance); (b) URANS (RMS) (c) URANS (Variance)

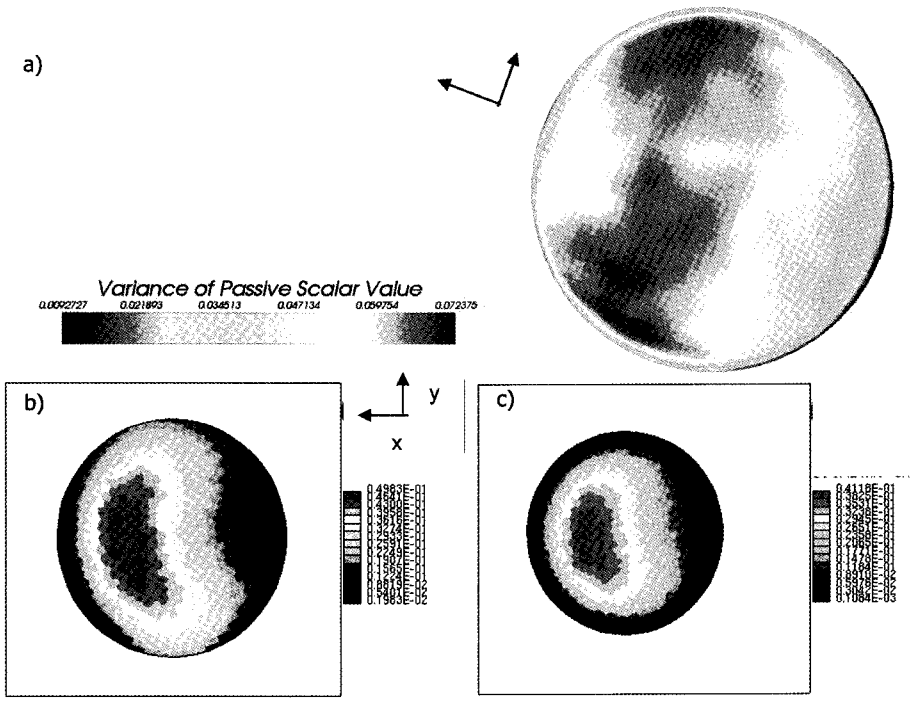

Fig. 13. Variance of the Passive Scalar on Measurement Plane 4: (a) LES (Variance); (b) URANS (Variance); (c) URANS (Coherent Part of the Variance)

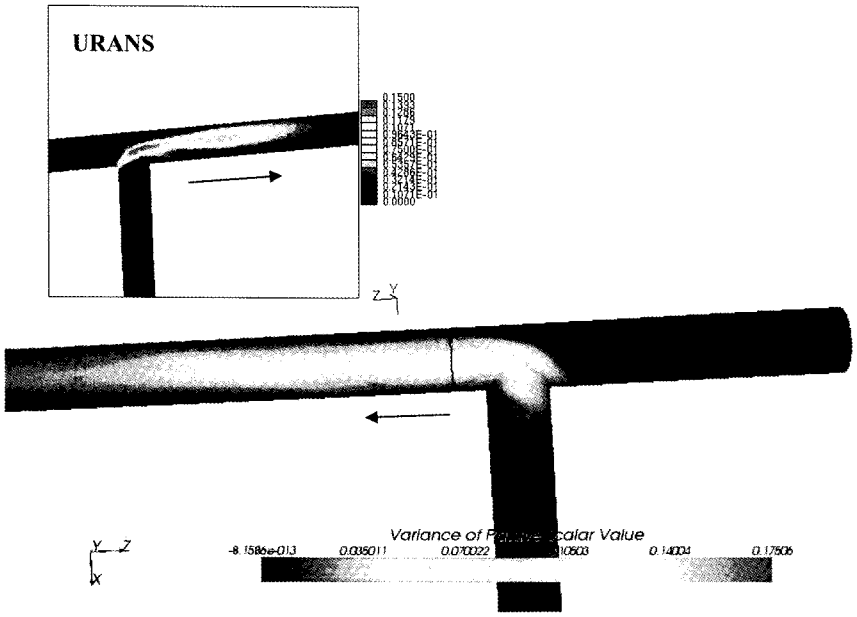

Fig. 14. Variance of the Passive Scalar on the Wall Surface, URANS and LES

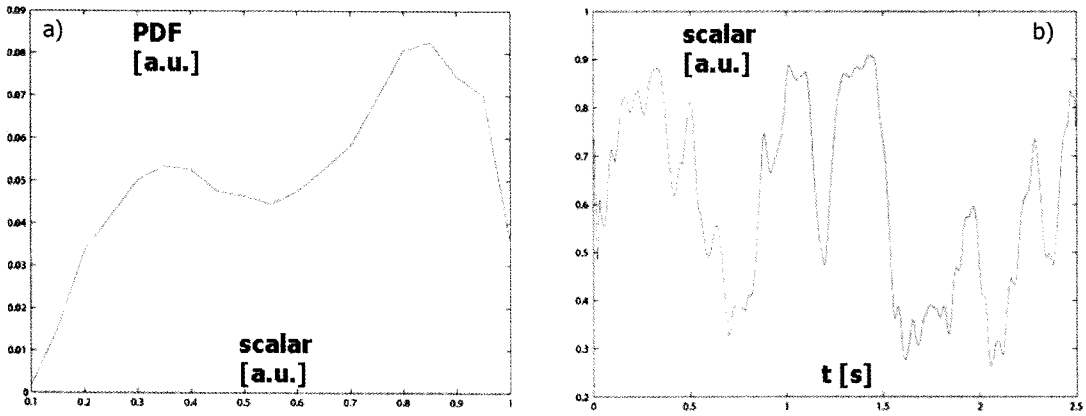

Fig. 15. Monitoring Point Positioned at the Peak of the RMS (Fig. 10): (a) Probability Density Function of the Passive Scalar; (b) Time History of the Passive Scalar

components of the RMS are included. The ratio between the coherent component and the total variance in (8) is shown in Fig. 10b and Fig. 11b. It can be seen in these figures that, in the peak region, the coherent part never exceeeds 45 % of the total variance. Any implementation of URANS which disregarded one of the components would immediately feature an error on the variance of 45 % (by a steady state calculation, for example) or 55 % (by not simulating the equation for the variance of the scalar).

3.4 Time Series

Figure 15 shows the time history of the passive scalar at a monitoring point fixed on the peak of the RMS in Fig. 10 (measurement plane 1, symmetry line). The time history is qualitatively comparable to the one published by Walker *et al.* [20] for the same case, even if the amplitude of the oscillations appears to be smaller (consistently with what was discussed in the introduction). It is interesting to notice that the probability density function for the passive scalar at this point presents two separate peaks (the asymmetry is due to the short integration time). The spectrum for the signal is shown in Fig. 16, and it is qualitatively comparable to the experimental behaviour. In fact, the solid lines on top of the graph (with the frequency dependencies of $f^{-1.7}$ and $f^{-0.75}$) approximate the experimental spectrum. It can be seen in the figure

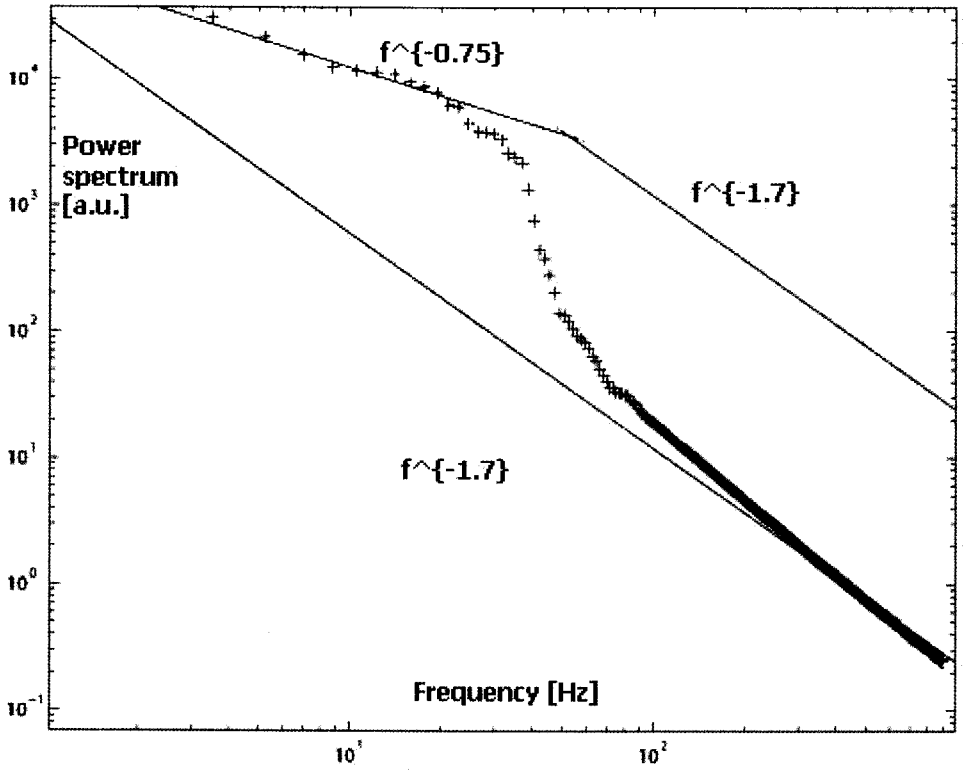

Fig. 16. Spectrum of the Passive Scalar: Monitoring Point Positioned at the Peak of the RMS (Fig. 10).

that the low-frequency, high-energy (up to 100 Hz) part of the spectrum is properly reproduced, while the high-frequencies are somehow dumped (in the range 100 Hz - 1000 Hz). This is an inherent limitation of URANS, consistent with theoretical expectations (i.e., the high frequency behaviour is filtered by the ensemble operator).

4. CONCLUSIONS

Simulation of the flow in a T-junction has been carried out here using the Unsteady Reynolds Averaged Navier-Stokes approach. A scalar equation has been solved to model the mixing in the junction region. This model corresponds to the mixing of a hot fluid and a cold fluid whenever buoyancy plays a marginal role. The URANS methodology was able to reproduce, at least qualitatively, the instantaneous flow field. The averaged flow field was in good agreement with an independent LES calculation up to four diameters downstream of the junction.

If a steady state RANS calculation is carried out, the passive scalar distribution, representative of the temperature of the fluid, tends to underestimate the mixing downstream and grossly underpredicts the RMS of the passive scalar representative of the temperature fluctuation. URANS results show a clear improvement, which starts to be evident 91 mm downstream of the junction.

Moreover, it has been demonstrated that without including an additional transport equation for the variance of the scalar, URANS is unable to predict the correct value of the RMS of the scalar. This result is relevant to the prediction of thermal fatigue, since the RMS of the temperature in the near wall regions of the pipe is an important physical parameter.

Future works should consider an investigation of the effects of turbulence modeling on the development of coherent structures downstream of the junction and should consider the effects of those coherent structures on mixing.

APPENDIX A

In this appendix, the Baglietto-Ninokata [10] model will be briefly presented. A complete description of the anisotropic k-ε formulation adopted for this work is available in Baglietto and Ninokata [10]. A cubic formulation is employed for stress-strain correlation (1.3), while the usual transport equations for the turbulent energy k and the turbulent dissipation rate ε are adopted, as in the classic model by Launder [21]. In contrast with the standard model, the adopted approach respects the constraint of realizability following the example of Lumley [22], and this is reflected in the fact that the C_μ coefficient is not formulated as a constant but instead is given as function

Table 1. Coefficients of the Non-linear Model[1]

c_{NL1}	c_{NL2}	c_{NL3}	c_{NL4}	c_{NL5}	c_{NL6}	c_{NL7}	c_{NL8}	c_{NL9}
0.8	11	4.5	-2.2	2.0	1000	1.0	15.0	8.0

[1] Please note that these coefficients refer to the STAR_CD implementation. Due to a slightly different implementation of the C_4 and C_5 coefficients, C_{NL4} and C_{NL5} become respectively -5 and -4.5 in STAR-CCM+.

of the shear invariant S:

$$C_\mu = \frac{2/3}{A_1 + S}, \tag{A1}$$

with:

$$S = \frac{k}{\varepsilon}\sqrt{\frac{1}{2}S_{ij}S_{ij}}, \tag{A2}$$

with a coefficient $A_1 = 3.9$.

The formulation of the coefficients in (1.3) multiplies the non-linear terms and respects the realizability conditions:

$$C_1 = \frac{c_{NL1}}{\left(c_{NL6} + c_{NL7}S^3\right)C_\mu}, \tag{A3}$$

$$C_2 = \frac{c_{NL2}}{\left(c_{NL6} + c_{NL7}S^3\right)C_\mu}, \tag{A4}$$

$$C_3 = \frac{c_{NL3}}{\left(c_{NL6} + c_{NL7}S^3\right)C_\mu}, \tag{A5}$$

$$C_4 = \frac{c_{NL4}}{\left(c_{NL8} + c_{NL9}S + S^2\right)}, \tag{A6}$$

$$C_5 = \frac{c_{NL5}}{\left(c_{NL8} + c_{NL9}S + S^2\right)}, \tag{A7}$$

and the adopted coefficients c_{NL1}, c_{NL2}, c_{NL3}, c_{NL4} ... c_{NL9} are given in Table 1. Moreover, the turbulent viscosity is given by the following equation:

$$\mu_t = f_\mu \frac{C_\mu \rho k^2}{\varepsilon}, \tag{A8}$$

where f_μ is a damping function. The wall is treated with a Low Reynolds number approach.

REFERENCES

[1] T. Kawamura et al., "Experimental study on thermal striping in mixing tees with hot and cold water", *ICONE 10*, April 14-18, 2002

[2] N. Fukushima, K. Fukugata, N. Kasagi, H.Noguchi, K. Tanimoto, "Numerical and Experimental Study on Turbulent Mixing in a T-junction Flow", *6th Joint ASME-JSME Thermal Engineering Joint Conference*, March 16-20, 2003

[3] A.K. Kuczaj, B. de Jager and E. Komen, "An assessment of Large-Eddy Simulation for thermal fatigue Prediction", *ICAPP'08*, United States, 2008

[4] Hu, L.W., Kazimi, M.S., "Large Eddy Simulation of Water Coolant Thermal Striping in a Mixing Tee Junction," *NURETH-10*, Seoul, Korea, October 5-9, 2003

[5] J. Westin et al. "Experiments and Unsteady CFD-Calculations of Thermal Mixing in a T-Junction", *CFD4NRS*, Garching, 5-7 September, 2006

[6] H. Ha Minh, "La Modélisation Statistique de la Turbulence: Ses Capacités et ses Limitations", *Comptes rendu de l'Academie des Sciences*, **327**, pp. 343-358 (1999)

[7] E. Merzari, E. Baglietto and H. Ninokata, «LES simulation of the flow in a T-junction», ICAPP'09, Tokyo, Japan, May 11th - May 15th 2009

[8] A. Smirnov, S. Shi and I. Celik. "Random Flow Generation Technique for Large Eddy Simulations and Particle-Dynamics Modeling." *Trans. ASME. Journal of Fluids Engineering*, **123**, 359-371 (2001)

[9] R. Zboray, A. Manera, B. Niceno and H.M. Prasser, "Investigations on Mixing Phenomena in Single-Phase Flows in a T-junction Geometry", *Nureth-12*, Pittsburgh, USA Sept. 30-Oct. 4, 2007

[10] E. Baglietto and H.Ninokata, "Anisotropic Eddy Viscosity Modeling for Application in Industrial Engineering Internal Flows", *Int. J. Transport Phenomena*, **8** (2006)

[11] J. Hsieh, F. S. Lien and E. Yee, "Numerical modeling of passive scalar dispersion in an urban canopy layer", *Journal of Wind Engineering and Industrial Aerodynamics*, **95**, 1611 (2007)

[12] Z. Warhaft, "Passive scalars in turbulent flows", *Annu. Rev. Fluid Mech.*, **32**, 203-240 (2000)

[13] STAR-CCM+ 2.10 User guide

[14] STAR-CD 4.06 Methodology Guide

[15] R.I. Issa, "Solution of the implicitly discretised fluid flow equations by operator-splitting", *J. Comp. Phys.*, **Vol. 62**, pp. 40–65 (1986).

[16] P.R. Spalart and S. R. Allmaras, "A one-equation turbulence model for aerodynamic flows", 30th AIAA Aerospace Sciences

Meeting and Exhibit, Reno, NV; United States; 6-9 Jan. 1992.
[17] Craft, T.J., Launder, B.E., and Suga, K. 1993. 'Extending the applicability of eddy viscosity models through the use of deformation invariants and non-linear elements", Proc. 5th Int. Symp. on Refined Flow Modelling and Turbulence Measurements, pp. 125-132
[18] J. Hunt, A. A. Wray, P. Moin, "Eddies, Streams and convergence zones in turbulent flows", Report CTR-S88, Center for turbulence Research - Stanford university (1988)
[19] Th. Frank, M. Adlakha, C. Lifante, H.-M. Prasser, F. Menter, "Simulation of Turbulent and Thermal Mixing in T-Junctions Using URANS and Scale-Resolving Turbulence Models in ANSYS CFX", *CFD4NRS*, Grenoble, 2008
[20] C. Walker, M. Simiano, R. Zboray and H.-M. Prasser, "Investigations on mixing phenomena in single-phase flow in a T-junction geometry", *Nuclear Engineering and Design*, **239**, 116-126 (2009)
[21] B.E. Launder and D.B Spalding, "The numerical computation of turbulent flows", *Comp. Meth. in Appl. Mech. and Eng.*, **3**, 269-289 (1974)
[22] J. L. Lumley, "Toward a turbulent constitutive relation", *J. Fluid Mechanics*, **41**, 413-434 (1970)